8.

Mathematical modelling and investigations of the hexapod robot

8.1. Introduction

Legged locomotion is the most common locomotion form in nature which is used by numerous animal species in order to move on the Earth. It motivated and became the inspiration for many researchers for the construction of walking machines which belong to the most important group of mobile robots met in engineering applications. There are numerous examples of both biological inspirations and constructed prototypes of multi-legged robots (including hexapod robots) investigated. Interesting state-of-the-art in this area can be found in papers [8.5, 8.12]. In particular, in reference [8.12] a summary of biological paragon from nature, methods of investigations of legged locomotion and the constructed multi-legged robots are presented and discussed.

Investigations of multi-legged robots have been initiated in 1960s by McGhee and Frank [8.17], who constructed the first four-legged robot called 'Phoney Pony'. Since that time a wide variety of four-legged (quadruped) robots have been built, including: TITAN-VIII [8.1] - the robot driven by wire-pulley system; BISAM [8.2] - the self-adaptive quadruped robot; SIL04 [8.11] - the robot driven by DC servomotor with torus worm gear; Tekken [8.10] - the robot controlled by the system including CPG and reflection mechanism; ARAMIES [8.22] - the robot for working in non-structural environment, and BigDog [8.20] - the robot constructed for transport of military materials.

One of the most important issues regarding the legged robots are contact forces between robot leg tips and the ground which should be taken into account when the robot locomotion is planned on the unknown terrain. The second important issue related to the mobile walking robots is their energy consumption during walking. This is why during three last decades different types of hexapod walking robots (and also other multi-legged machines) have been constructed, modified and analytically/experimentally investigated in order to reduce their energy consumption [8.15, 8.18].

The literature review shows that walking machines, especially hexapod robots due to their great stability during walking, are still objects of studies of

many researchers. In engineering calculations, the appropriate mathematical models of different kinds of robots are rarely used since engineers usually employ commercial software - such as Sim Mechanics or Adams. This is why one of the main goals of this chapter is to take into account the mentioned problem by adopting the appropriate dynamic model with kinematic excitation of the robot legs and focusing on the contact forces acting along the vertical direction (along the gravity field). Minimization of the mentioned energy consumption extends time of the robot operation which often plays a key role in carrying out the mission. Since the legged robots are the most commonly used and constructed walking machines, the proposed methods and results can be adopted to a wide group of mobile robots reported in the literature.

8.2. The prototype of the constructed hexapod robot

8.2.1. Biological inspiration

Usually each insect leg is made up of five basic segments connected by joints, namely: Coxa, Trochanter, Femur, Tibia, and Tarsus [8.3]. However, in the literature the mechanisms having 3-DOF modeling hexapod legs usually can be found, since the mentioned additional DOFs are rarely used in a typical walking process. Following the results reported in papers [8.9] and [8.21], similar schematic diagram of a morphology of a stick insect leg is taken into account (see Fig. 8.1). Coxa, Femur and Tibia lie approximately in a plane (referred as a leg plane). Moreover, in engineering prototypes of the robots usually Tarsus segments are ignored.

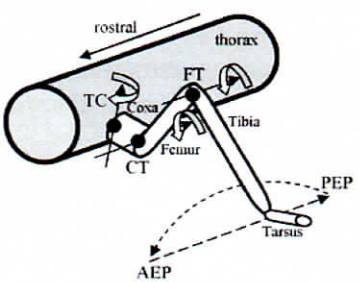

Fig. 8.1. Scheme of a typical stick insect leg with four functional segments: Coxa (Cx), Femur (Fe), Tibia (Ti) and Tarsus (Ta)

TC describes the angle position of the Thorax-Coxa joint, CT denotes the angle position of the Coxa-Trochanterofemur joint, whereas FT is the angle position of the Femur-Tibia joint [8.9, 8.21]. The single stride cycle of the

walking leg (the dashed line in Fig. 8.1) can be regarded as being in one of two functional states, either a swing movement (also referred as a return stroke) or a stance movement (also referred as a power stroke). The mentioned two phases of leg movement are mutually exclusive - it means that leg cannot be in swing state and in stance state at the same time. The point PEP denotes the posterior extreme position of the leg, while the point AEP denotes the anterior extreme position of the leg.

8.2.2. Mechanism of the robot leg

In numerous engineering applications usually robot legs with only three segments (Coxa, Femur and Tibia) are developed (see papers [8.3, 8.4, 8.8, 8.16] and others). This is why also in this chapter the additional and rarely used by insects DOFs are neglected, and therefore three-joint leg mechanism of the constructed robot is considered. On the basis of the schematic diagram of an insect leg presented above, kinematic model, CAD view and constructed prototype of the robot leg are considered and illustrated in Fig. 8.2.

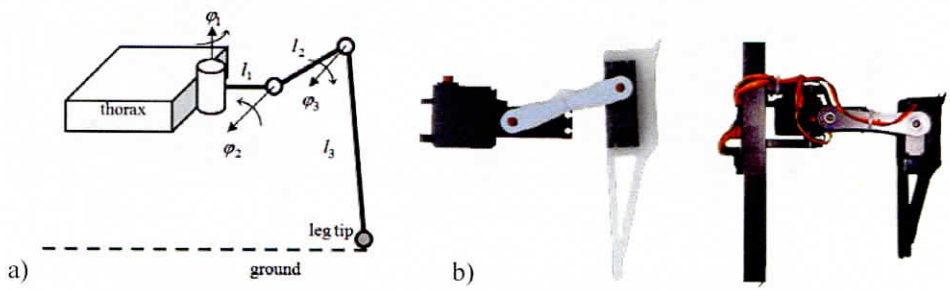

Fig. 8.2. Leg of the hexapod robot: a) the kinematic structure, b) the CAD design, c) the constructed prototype

The angle $\varphi_1 = 45° ... 135°$ corresponds to the angular position of the Thorax-Coxa joint (TC joint), the angle $\varphi_2 = -90° ... 90°$ corresponds to the angular position of the Coxa-Trochanterofemur joint (CT joint), while the angle $\varphi_3 = 0° ... 150°$ corresponds to the angular position of the Femur-Tibia joint (FT joint). In order to control the robot legs the electric actuators Tower Pro Mg995 possessing a servo feedback and proportional controller are used which are controlled via PWM (Pulse-Width Modulation) technique. The lengths of the three straight line links (which corresponds to the Coxa, Femur and Tibia) are equal $l_1 = 27$ mm, $l_2 = 70$ mm and $l_3 = 120$ mm, respectively. Changes in all leg stiffness are neglected.

8.2.3. General presentation of the constructed robot

Figure 8.3 shows CAD model created in the Inventor software and a photo of the constructed prototype of the hexapod robot. The illustrated CAD model is well suited for design changes and optimization as well as for virtual experiments of the robot movements. The constructed robot can be used for experimental investigations regarding kinematic parameters of the robot locomotion, contact forces between the robot legs and the ground, and its power consumption. The mechanical construction consists of two main components, i.e. the body which houses electronic circuits, and six identical legs driven by eighteen servomotors. Most of the remaining mechanical elements of the robot have been made using a 3D printer. The full size of the robot is about 400 mm x 380 mm 220 mm (length × width × height) with an additional ground clearance during standing. The robot weights over 2 kg and can move at maximum speed of about 0.6 kilometer per hour.

a) b)

Fig. 8.3. Studied hexapod robot: a) CAD model created in Inventor, b) constructed prototype

The control system of the robot consists of a number of distinct modules which are responsible for solving particular subtasks. Data from the sensors installed on the robot are processed by the ARM (Advanced RISC Machine) microcontroller and transmitted to the mobile phone using wireless network (BTM-222 module). Similarly works communication to the opposite direction, namely transmission of control signals (for instance different parameters of the robot gait) from the mobile phone to the microcontroller. Generation of the angular positions for the individual servos installed in the robot legs using CPGs is discussed later in Section 8.4.3.

8.3. Mathematical modelling of the hexapod robot

8.3.1. Direct and inverse kinematics of the robot leg

The kinematic scheme of the considered robot leg in the body reference frame coordinate system xyz for arbitrary configuration is shown in Fig. 8.4a. In order to obtain relations for the inverse kinematics of the robot leg we take into account the mechanism of the robot leg lying in the leg plane (see Fig. 8.4b).

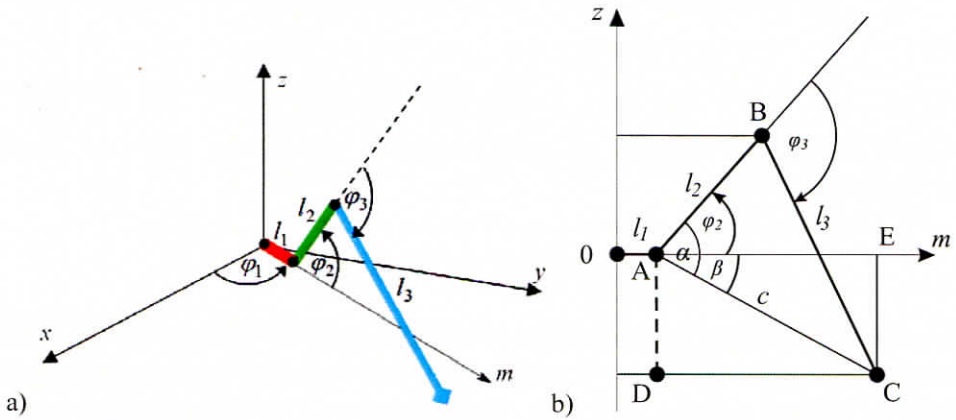

Fig. 8.4. Kinematical model of a robot leg: a) a robot leg located in the body reference frame, b) projection of the considered robot leg on the leg plane $z-m$ defined by the mechanism of the leg

The direct kinematics can be determined by taking coordinates x, y and z (the leg tip positions in the body reference frame) as a function of the lengths l_1, l_2, l_3 and the angles φ_1, φ_2, φ_3 in the form

$$\begin{cases} x = \cos\varphi_1(l_1 + l_2\cos\varphi_2 + l_3\cos(\varphi_3 - \varphi_2)), \\ y = \sin\varphi_1(l_1 + l_2\cos\varphi_2 + l_3\cos(\varphi_3 - \varphi_2)), \\ z = l_2\sin\varphi_2 - l_3\sin(\varphi_3 - \varphi_2). \end{cases} \tag{8.1}$$

In turn, the relationships for inverse kinematics have the following form

$$\varphi_1 = \begin{cases} \arctan(y/x) & \text{if} \quad x > 0, \\ \pi/2 & \text{if} \quad x = 0, \\ \pi - \arctan(y/(-x)) & \text{if} \quad x < 0, \end{cases} \tag{8.2}$$

$$\varphi_2 = \begin{cases} \alpha + \beta & \text{if} \quad \sqrt{x^2 + y^2} - l_1 \geq 0, \\ \alpha - (\pi - \beta) & \text{if} \quad \sqrt{x^2 + y^2} - l_1 < 0, \end{cases} \tag{8.3}$$

$$\varphi_3 = \arccos\left(\frac{c^2 - l_2^2 - l_3^2}{2 l_2 l_3} \right), \tag{8.4}$$

where $\alpha = \arccos\left(\dfrac{l_3^2 - l_2^2 - c^2}{-2 l_2 c} \right)$, $\beta = \arctan\left(\dfrac{z}{\sqrt{x^2 + y^2} - l_1} \right)$,

and $c = \sqrt{z^2 + \left(\sqrt{x^2 + y^2} - l_1 \right)^2}$. The obtained relationships for direct and inverse kinematics are used in both numerical simulations and real control system of the robot.

8.3.2. Dynamical model of the robot with tripod gait

Figure 8.5 shows a model of the considered hexapod robot embedded in the gravity field with coefficient $g = 9{,}81\,\mathrm{m/s^2}$ and supported by three legs which form the support polygon. The mass of the robot body (without limbs) is equal to $M_B = 2.00\,\mathrm{kg}$ and its six identical legs are denoted as L1, L2, L3 (on the left side of the robot) and R1, R2, R3 (on the right side of the robot).

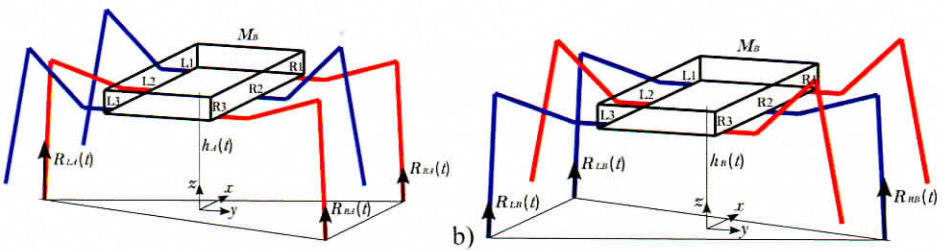

Fig. 8.5. Model of the hexapod robot with tripod gait configuration:
a) the robot supported by the legs R1, R3 and L2,
b) the robot supported by the legs L1, L3 and R2

Each of the robot legs contains three links with masses $m_1 = 0.12\,\mathrm{kg}$, $m_2 = 0.05\,\mathrm{kg}$ and $m_3 = 0.15\,\mathrm{kg}$, respectively. In the case of the tripod gait, the legs of the robot can be divided into two groups, i.e. the group A (solid legs R1, R3 and L2) and group B (dashed legs L1, L3 and R2). The movements of all robot legs are controlled by the same CPG, however, the signals applied to the

group B of the legs (joint angles $\varphi_{1B}(t)$, $\varphi_{2B}(t)$ and $\varphi_{3B}(t)$) are in anti-phase with respect to signals applied to the group A (joint angles $\varphi_{1A}(t)$, $\varphi_{2A}(t)$ and $\varphi_{3A}(t)$). Due to symmetry of the considered system it can be assumed that the contact forces in legs L1 and L3 are the same. Moreover, the contact forces in legs R1 and R3 are also the same. In the case of the robot walking on a relatively hard ground, it can be assumed that there is no rotation of the robot body, and therefore the corresponding rotational movements and moment of inertia of the robot body can be neglected. The coordinates of the gravity centres of the individual links of the robot legs can be expressed in the following way

$$z_{1RA}(t) = z_{1LA}(t) = z_{1RB}(t) = z_{1LB}(t) = z_C(t), \tag{8.5}$$

$$z_{2RA}(t) = z_{2LA}(t) = z_C(t) + a_2 \sin\varphi_{2A}(t), \tag{8.6}$$

$$z_{2RB}(t) = z_{2LB}(t) = z_C(t) + a_2 \sin\varphi_{2B}(t), \tag{8.7}$$

$$z_{3RA}(t) = z_{3LA}(t) = z_C(t) + l_2 \sin\varphi_{2A}(t) - a_3 \sin(\varphi_{3A}(t) - \varphi_{2A}(t)), \tag{8.8}$$

$$z_{3RB}(t) = z_{3LB}(t) = z_C(t) + l_2 \sin\varphi_{2B}(t) - a_3 \sin(\varphi_{3B}(t) - \varphi_{2B}(t)), \tag{8.9}$$

where in our construction a_1 =13.5 mm, a_2 = 35 mm, a_3 = 40 mm. Position of the robot gravity centre $z_C(t)$ in the considered Cartesian coordinate system can be obtained from the following relation

$$z_C(t) = \begin{cases} h_A(t) & \text{dla} \quad h_A(t) \geq h_B(t), \\ h_B(t) & \text{dla} \quad h_A(t) < h_B(t), \end{cases} \tag{8.10}$$

where

$$z_{1RA}(t) = z_{1LA}(t) = z_{1RB}(t) = z_{1LB}(t) = z_C(t), \tag{8.11}$$

$$z_{2RA}(t) = z_{2LA}(t) = z_C(t) + a_2 \sin\varphi_{2A}(t). \tag{8.12}$$

As a result, equations for translatory motion in the vertical direction z can be written in the following form

$$\begin{aligned} &M_B \ddot{z}_C(t) + 2\sum_{i=1}^{3} m_i \ddot{z}_{iRA}(t) + \sum_{i=1}^{3} m_i \ddot{z}_{iLA}(t) + 2\sum_{i=1}^{3} m_i \ddot{z}_{iLB}(t) + \\ &+ \sum_{i=1}^{3} m_i \ddot{z}_{iRB}(t) = 2R_{RA}(t) + R_{LA}(t) - \left(6\sum_{i=1}^{3} m_i + M_B\right) g \end{aligned} \tag{8.13}$$

if $h_A(t) \geq h_B(t)$ (see Fig. 8.5a), or

$$M_B\ddot{z}_C(t)+2\sum_{i=1}^{3}m_i\ddot{z}_{iRA}(t)+\sum_{i=1}^{3}m_i\ddot{z}_{iLA}(t)+2\sum_{i=1}^{3}m_i\ddot{z}_{iLB}(t)+$$
$$+\sum_{i=1}^{3}m_i\ddot{z}_{iRB}(t)=2R_{LB}(t)+R_{RB}(t)-\left(6\sum_{i=1}^{3}m_i+M_B\right)g \tag{8.14}$$

if $h_A(t)<h_B(t)$ (see Fig. 8.5b). Taking into account symmetrical distribution of the robot legs and partial compensation of their mutual movements, it can be assumed that $R_{LA}(t)=2R_{RA}(t)$ and $R_{RB}(t)=2R_{LB}(t)$.

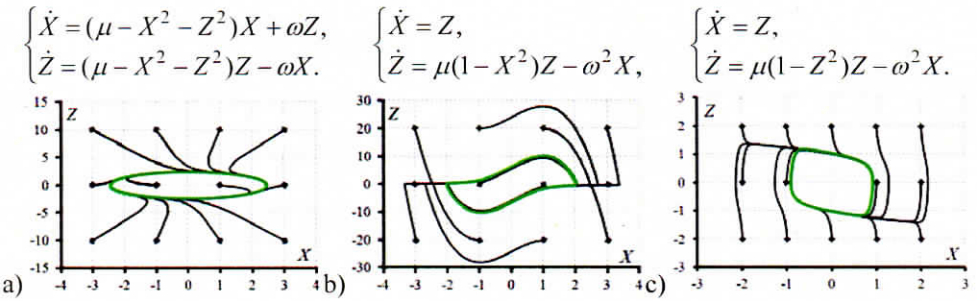

Fig. 8.6. Equations of motion and phase trajectories of the three typical nonlinear oscillators for $\omega=2$, $\mu=6$ and different initial conditions marked with black squares (green bolded lines indicate stable trajectories): a) Hopf oscillator, b) van der Pol oscillator, c) Rayleigh oscillator

8.4. Control of the robot using Central Pattern Generators

8.4.1. Literature review

There are a lot of scientific papers devoted to the method of gait generation which includes the method based on CPGs (for instance, see papers [8.7, 8.23, 8.24]). The first CPG model was proposed by Cohen, Holmes and Rand in 1980s through the study on the dissection of a lamprey spinal cord [8.6]. Since that time, numerous linear and nonlinear oscillators with stable orbits have been used and applied as a CPG models, including damped or un-damped harmonic oscillators, van der Pol and Rayleigh oscillators, Toda-Rayleigh lattice and others [8.19]. A brief state-of-the-art devoted to the implementation of CPG algorithms for control hexapod motion is presented in [8.4] and in the review paper [8.14]. In this chapter we used a relatively simple control system based on the CPG. However, in contrast to the previous work found in the literature, new CPG model is proposed. As a typical mechanical oscillators form literature working as a CPGs, three popular and well known nonlinear oscillators are taking into

consideration, namely: Hopf oscillator, van der Pol oscillator and Rayleigh oscillator. Ordinary differential equations and stable trajectories of the mentioned oscillators are reported in Fig. 8.6. The presented trajectories oscillate stably regardless of the initial conditions and therefore they are often used to generate the trajectory of a leg tip of robot legs. The obtained in this way trajectories cannot be directly used to control the robot legs. First, they must be converted to the workspace of the leg mechanism and then to the joints space of the leg by using inverse kinematics rules.

8.4.2. Stick-slip oscillator as a CPG

Motivated by the carried out study of a trajectory of a leg tip of real insects and various biologically inspired robots, other 1-DOF nonlinear mechanical oscillator with stick-slip induced vibrations is employed in this chapter as a novel model of CPG. The trajectory of stable orbit of the proposed CPG (after inverting with respect to the coordinates axes) looks like the shape of the trajectory of a leg tip of a stick insect presented in Fig. 8.1. The proposed model is governed by the following non-dimensional first order ordinary differential equations

$$\begin{cases} \dot{X} = Z, \\ \dot{Z} = -d_c Z - X + F_{fr}(v_r), \end{cases} \tag{8.15}$$

where d_c denotes the non-dimensional damping coefficient, and $F_{fr}(v_r) = \dfrac{F_s}{1+\delta|v_r|}\operatorname{sgn}(v_r)$ is the non-dimensional dry friction force depending on the non-dimensional relative sliding velocity $v_r = v_{dr} - \dot{X}$ with respect to the constant velocity v_{dr}. Parameters F_s and δ characterize function $F_{fr}(v_r)$. Non-continuous signum function $\operatorname{sgn}(v_r)$ is approximated by the smooth and often applied hyperbolic tangent function

$$\operatorname{sgn}(v_r) = \tanh\left(\frac{v_r}{\varepsilon}\right) \tag{8.16}$$

with numerical control parameter ε. Parameters d_c, v_{dr}, F_s and δ of the proposed model have a great impact on the frequency of vibrations and the shape of the obtained stable orbits. In further numerical simulations and experimental investigations we take into consideration stable trajectories of the proposed model obtained for the following initial parameters: $d_c = 0.01$, $F_s = 1.2$, $\delta = 3$, $v_{dr} = 0.5$ and the control parameter $\varepsilon = 10^{-4}$. As an example, Fig. 8.7

illustrates the obtained stable orbits for different parameter v_{dr} and different initial conditions.

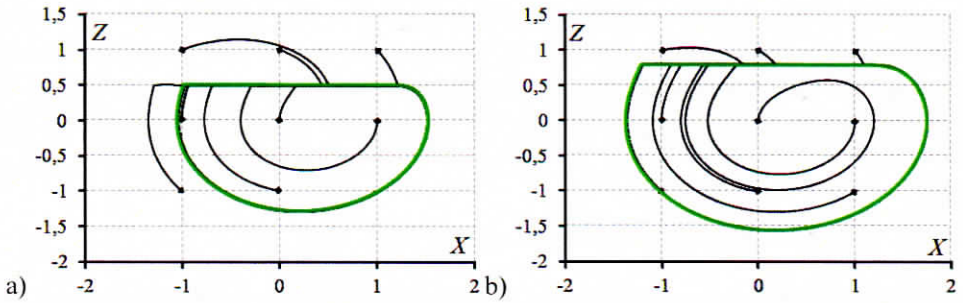

Fig. 8.7. Phase trajectories of the proposed CPG model for different initial conditions marked with black squares and green bolded lines as a stable trajectories: a) $v_{dr} = 0.5$, b) $v_{dr} = 0.8$

As can be seen, the trajectories presented in Fig. 8.7 oscillate stably (bolded green curves) regardless of the initial conditions and therefore they can be used to generate the trajectory of a leg tip of robot legs. Different shapes and periods of the stable orbits can be regulated by changing the parameters of the proposed CPG model.

8.4.3. Control structure of the robot leg movements

In our studies we use the following original method to control robot legs. First, the appropriate calculations of the stable orbits are started from initial condition which lies in the stable orbit and, as a result, we omitted transient states. Second, the obtained orbits (variables X and Z) are scaled by the normalization in such a way that the generated trajectories lie in the unit ranges: $X \in [-0.5,0.5]$ and $Z \in [0,1]$. Third, the period of the stable orbit is controlled by the software implemented in the microcontroller using the regulated time delays. Patterns of the stable orbits obtained in this way are shown in Fig. 8.8a. Next, multiplying the variables X and Z of an oscillator working as a CPG, we can directly change both the length and height of the robot stride. The example of the trajectory of CPG scaled in this way to the workspace of the robot leg mechanism is shown in Fig. 8.8b.

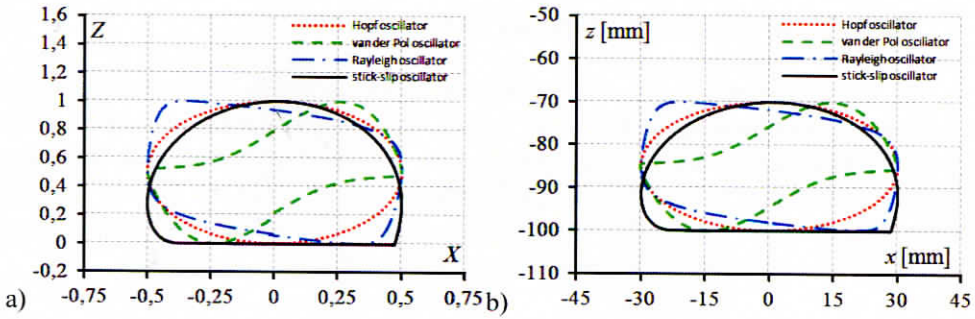

Fig. 8.8. Stable orbits of the CPGs: a) normalized periodic orbits, b) the same orbits converted into workspace of the leg mechanism for $l = 60$ mm and $h = 30$ mm

In the conducted numerical simulations and real control of the robot legs we use variable X of CPG to control the leg tip in the direction of the x-axis, variable $\dot{X} = Z$ to control the leg tip in the z direction, while the coordinate y of the leg tip is constant (in the considered robot we take $y = 110$ mm). In further studies we take into consideration only tripod gait for the considered robot locomotion, since this type of gait belongs to one of the most popular gaits, commonly used by both the six-legged insects and six-legged walking robots met in engineering applications. The method to generates signals (angle values) for each leg of the robot is presented schematically in Fig. 8.9.

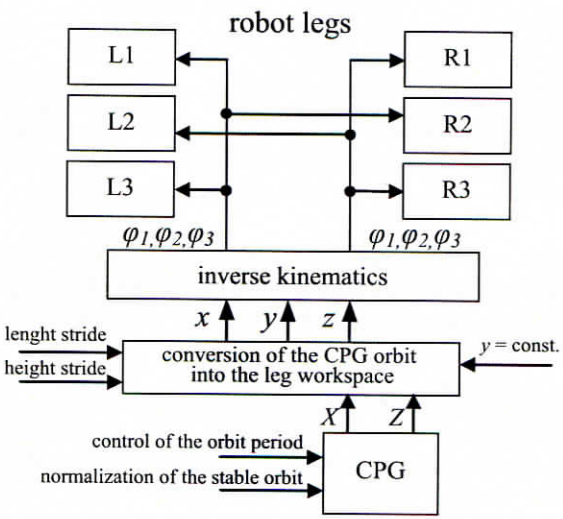

Fig. 8.9. Generation of angles values for each servo of the robot legs

8.5. Numerical simulations of the robot

In numerical simulations we used the standard fourth order Runge–Kutta method implemented in Scilab and Explicit-Runge–Kutta method implemented in Mathematica. Initial parameters of the considered robot gait are: the stride length equal to l =100 mm, the stride height equal to h = 40 mm and the stride period equal to T = 2 s . Numerical simulations of the considered robot have been also reported in our previous papers [8.12, 8.13].

8.5.1. Simulations of a single robot leg

Fig. 8.10 shows robot leg configurations with the stable trajectory plotted by the leg tip in regular time intervals. The presented numerical results show how the considered oscillators can be used to control the leg tip of the robot. In all cases the leg tip plots the stable trajectory in the workspace of the leg mechanism. Moreover, as expected, the mentioned plotted trajectories are limited to a two-dimensional plane which is parallel to the xz plane (y = const.).

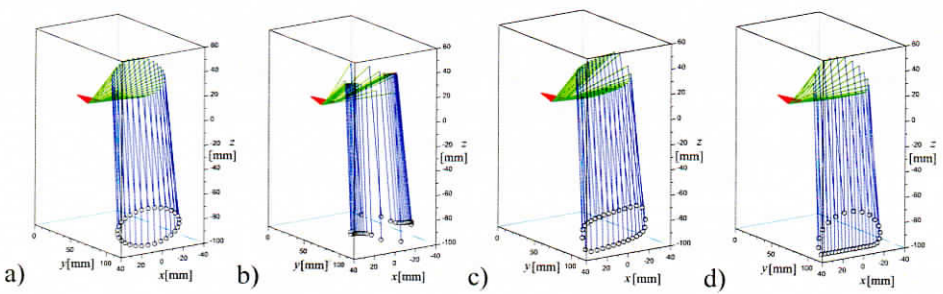

Fig. 8.10. Visualization of the robot leg configurations with the plotted stable trajectory regarding the leg tip: a) Hopf oscillator, b) van der Pol oscillator, c) Rayleigh oscillator, d) stick-slip oscillator

Fig. 8.11 shows comparison of the stable trajectory of the leg tip plotted for the proposed stick-slip oscillator as a CPG and the trajectory plotted by a leg tip of a real stick insect (presented earlier in Fig. 8.1). The leg tip of the robot starts from the initial configuration, finally plotting the stable trajectory in the workspace which lies in the plane parallel to the xz plane. The so-called 'slip phase' of the stick-slip vibrations (proposed CPG model) corresponds to the swing movement of the leg, and the so-called 'stick phase' of the mentioned stick-slip vibrations corresponds to the stance movement of the leg. Moreover, 'transition from stick to slip phase' corresponds to the posterior extreme position, whereas 'transition from slip to stick phase' corresponds to the anterior extreme position of the robot leg.

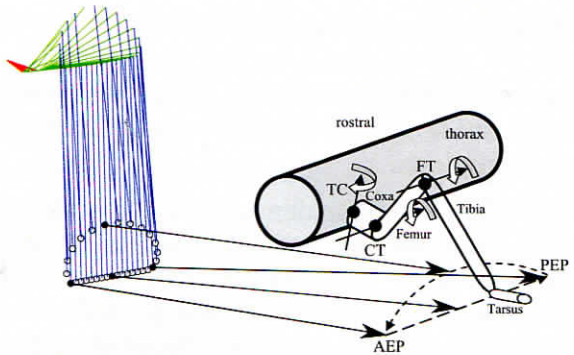

Fig. 8.11. Comparison of the stable trajectory of the leg tip plotted by using the proposed stick-slip oscillator with a trajectory plotted by a leg tip of a real stick insect

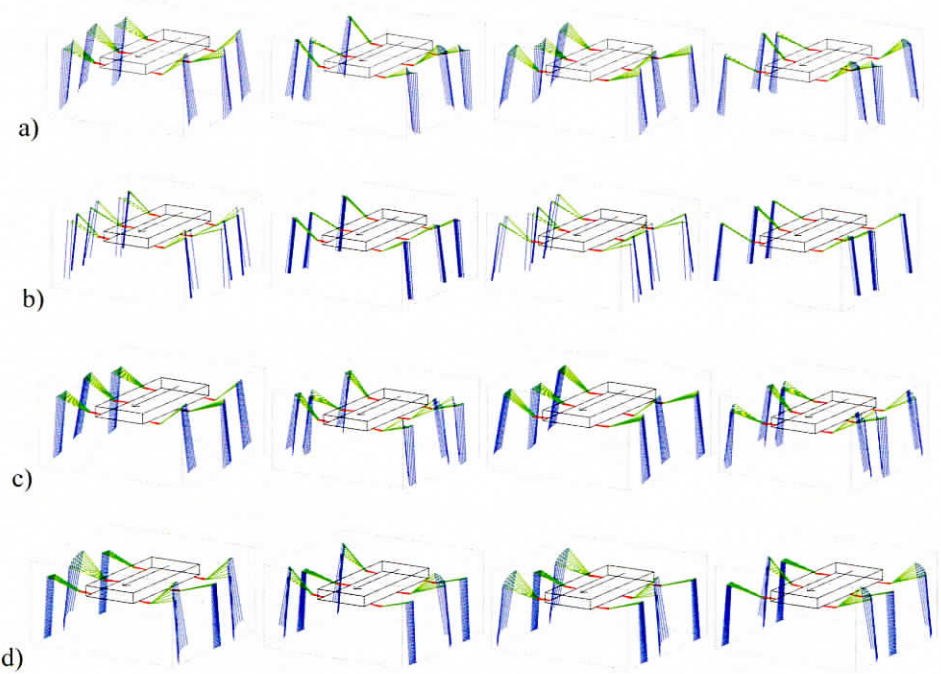

Fig. 8.12. Configurations of the robot legs plotted in regular time intervals in different equal phases of the single robot stride (from the left to the right) obtained numerically for different CPGs: a) Hopf oscillator, b) van der Pol oscillator, c) Rayleigh oscillator, d) stick-slip oscillator

8.5.2. Simulations of the whole robot

Fig. 8.12 shows configurations of all legs plotted in regular time intervals in four phases of single stride of the robot and for different CPGs (the arrow indicates the forward direction).

Through the analysis of configurations of individual legs it can be observed that, in cases of Hopf, van der Pol and Rayleigh oscillators, there exist such phases of the robot motion in which the distance between the centre of the coordinate system and the leg tips touching the ground changes significantly. Moreover, it can be seen that for van der Pol oscillator, some periods of the robot motion are realized faster, and other slower. Only in case of the proposed stick-slip oscillator working as a CPG, there are almost no fluctuations of the gravity centre of the robot in any phase of its movement.

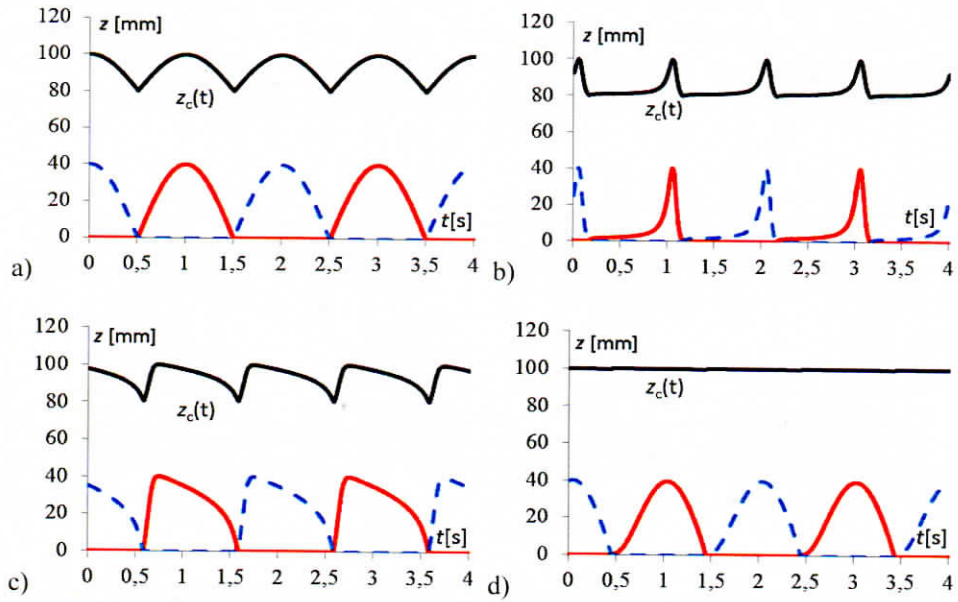

Fig. 8.13. Fluctuations of the robot gravity centre $z_C(t)$ and trajectories plotted by the robot legs for different CPGs (red solid curves - group A of the robot legs; blue dashed curves - group B of the robot legs): a) Hopf oscillator, b) van der Pol oscillator, c) Rayleigh oscillator, d) stick-slip oscillator

8.5.3. Kinematics of the whole robot

Fig. 8.13 shows the trajectories plotted by the gravity centre $z_C(t)$ of the robot in vertical direction and trajectories plotted by the tips of the robot legs

(group A - solid curves, and group B - dashed curves). When the three first oscillators controlling the robot legs are employed (Fig. 8.13a-c), on the contrary to the results presented in Fig. 8.13d, considerable fluctuations of the robot gravity centre are observed.

Figure 8.14 presents displacement curves of the robot gravity centre in both z and x direction obtained numerically for different CPGs. The adequate results regarding the velocity curves (obtained by numerical differentiation of the displacement curves) are presented in Fig. 8.15. Analysis of the results presented in Figs. 8.13-8.15 indicate that, in the cases of Hopf, van der Pol and Rayleigh oscillators, there exist such phases of the robot motion in which the distance between the centre of the coordinate system and the leg tips touching the ground changes significantly. Moreover, for the van der Pol oscillator, some periods of the robot motion are realized faster, while others slower. Only in the case of the stick-slip oscillator working as a CPG almost no fluctuations of the gravity centre of the robot in any phase of its movement are observed.

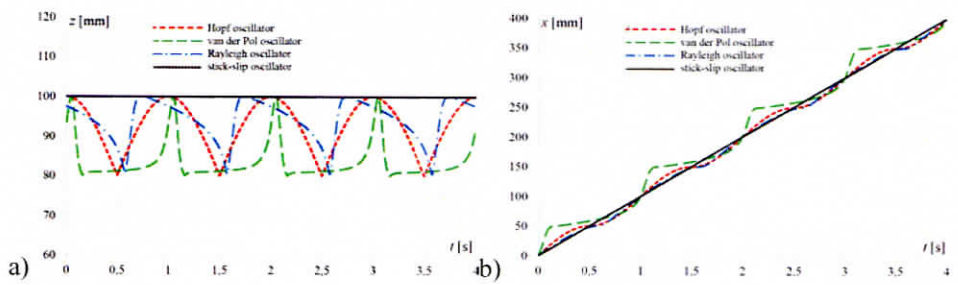

Fig. 8.14. Fluctuations of the displacement curves of the robot gravity centre obtained numerically for different CPGs: a) in z direction, b) in x direction

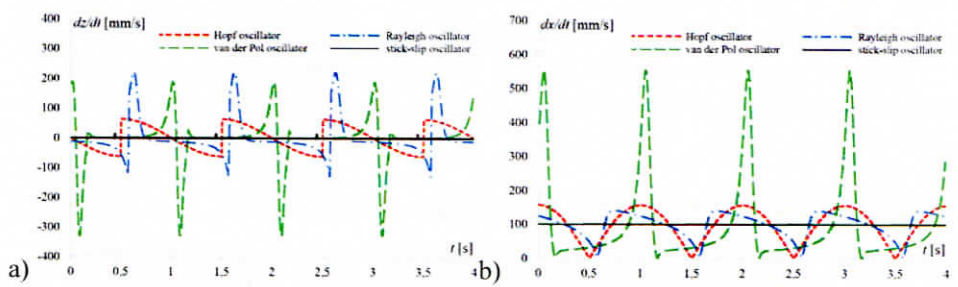

Fig. 8.15. Fluctuations of the velocity curves of the robot gravity centre obtained numerically for different CPGs: a) in z direction, b) in x direction

8.5.4. Contact forces of the robot

Figure 8.16 shows time histories of contact forces acting on the robot legs for different CPGs. The largest contact reaction forces between the legs and the ground occur in the central legs (i.e. L2 and R2) and this is why only these reactions are presented (the appropriate reaction forces in the lateral robot legs are two times smaller). As can be seen, the appropriate reaction forces oscillate (increase and decrease) around the reaction force resulting from the weight of the robot (about 11 N), when none of the robot component is moved. Moreover, the most frequent oscillations of contact forces occur in the case of the van der Pol oscillator and the Rayleigh one. In turn, the lowest fluctuations of contact forces exist when the stick-slip oscillator is employed.

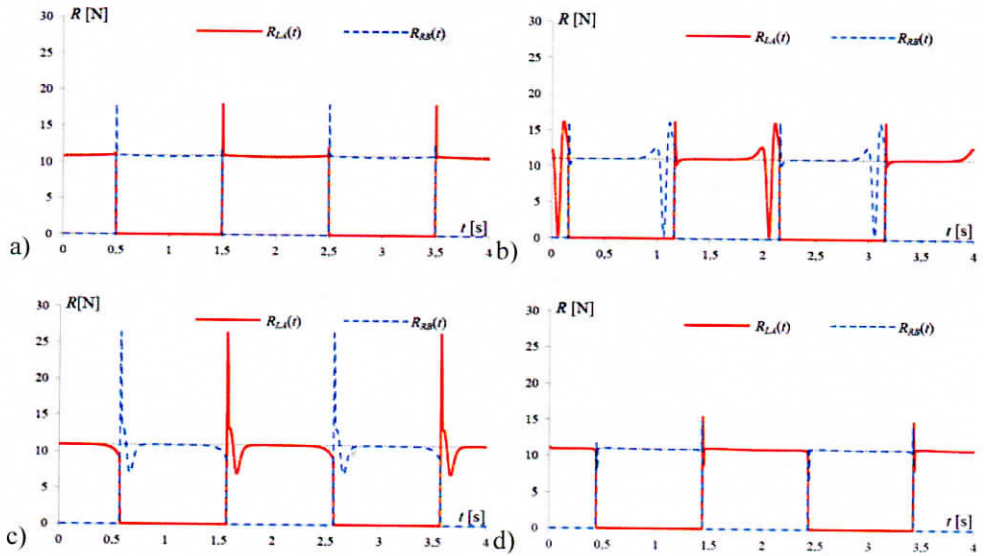

Fig. 8.16. Time histories of the reaction forces for the period of the single robot stride equal to 2 s (solid line denotes $R_{LA}(t)$, whereas dashed line denotes $R_{RB}(t)$):
a) Hopf oscillator, b) van der Pol oscillator, c) Rayleigh oscillator, d) stick-slip oscillator

8.6. Experimental investigations

Some obtained numerical simulations have been experimentally verified using the constructed prototype of the hexapod robot. Real fluctuations of the gravity centre of the robot have been obtained with the help of an optic sensor. Time histories of contact forces have been yielded by force sensors installed on the leg tips of the robot. In addition, experimental investigations of the average

power consumption and total energy demand have been carried out based on measurements of voltage and current data of individual servos installed in the joints of the robot legs with the help of a computer program created in LabView. During experimental measurement in all cases the obtained total distance covered by the robot was equal to 0.96 m. Experimental investigations of the constructed hexapod robot have been also reported in our previous papers [8.12, 8.13].

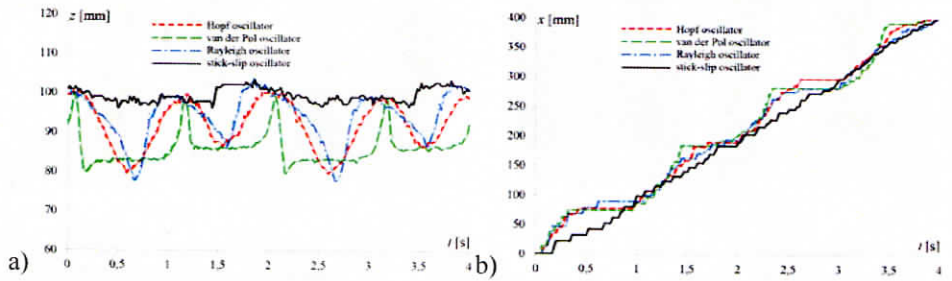

Fig. 8.17. Fluctuation of the displacement curves of the robot gravity centre obtained experimentally for different CPGs: in z direction, b) in x direction

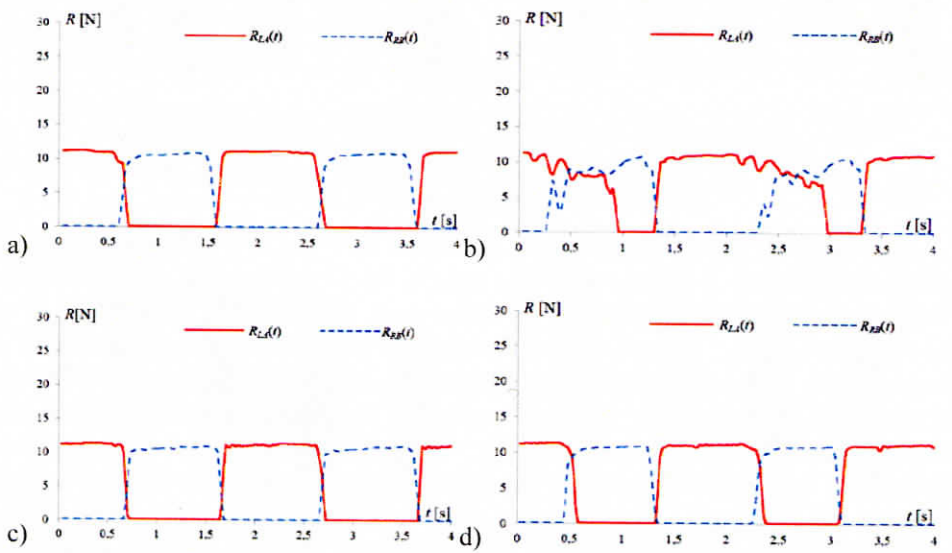

Fig. 8.18. Time histories of the reaction forces (red solid line denotes $R_{LA}(t)$, dashed blue line denotes $R_{RB}(t)$): a) Hopf oscillator, b) van der Pol oscillator, c) Rayleigh oscillator, d) stick-slip oscillator

Figure 8.17 shows the fluctuation curves of the gravity centre of the robot both in z and x direction. Time histories of contact forces between the robot legs and the ground are presented in Fig. 8.18. In turn, the average power

consumption and total energy cost analysis of the robot for different CPGs and for different gait parameters (stride length, stride height and stride period) are presented in Figs. 8.19 - 8.21.

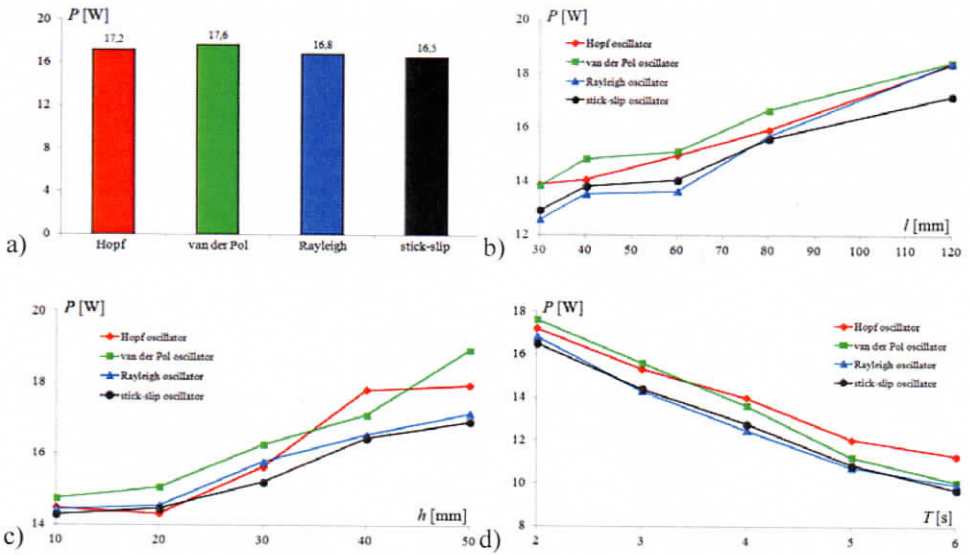

Fig. 8.19. Comparison of the average power consumption of the hexapod robot: a) for different CPG models, b) for different stride length l, c) for different stride height h, d) for different stride period T

The reported experimental results presented in Figs. 8.17-8.21 agree with the obtained numerical simulations. When we use the Hopf, the van der Pol and the Rayleigh oscillators, the robot gravity centre varies in the range of about a half of the stride height in z direction, and fluctuations of the robot gravity centre in x direction play also a significant role. In addition, it is clearly seen that in the case of stick-slip model, small changes regarding the mentioned fluctuations are observed, and it also agrees with the obtained numerical simulations. Time histories of contact reaction force between the legs of the robot and the ground obtained experimentally and shown in Fig. 8.18 are qualitatively similar to the numerical simulations shown in Fig. 8.16. However, the exact values of contact forces at the moment of changing of supporting legs are not detected in experimental investigations. Experimental results shown in Figs. 8.19-8.21 illustrate that both unnecessary variations of the gravity centre and acceleration/deceleration of the robot in the movement direction during walking have a negative impact on the average power consumption and total energy cost, since all servo mechanisms installed in robot legs must perform additional and unnecessary mechanical work. As it is numerically demonstrated and also

experimentally verified, the stick-slip model as a CPG does not possess these disadvantages and this is why in this case energy demand cost during walking of the robot is usually the smallest. It is particularly evident in Fig. 8.21, while the robot transports an extra mass.

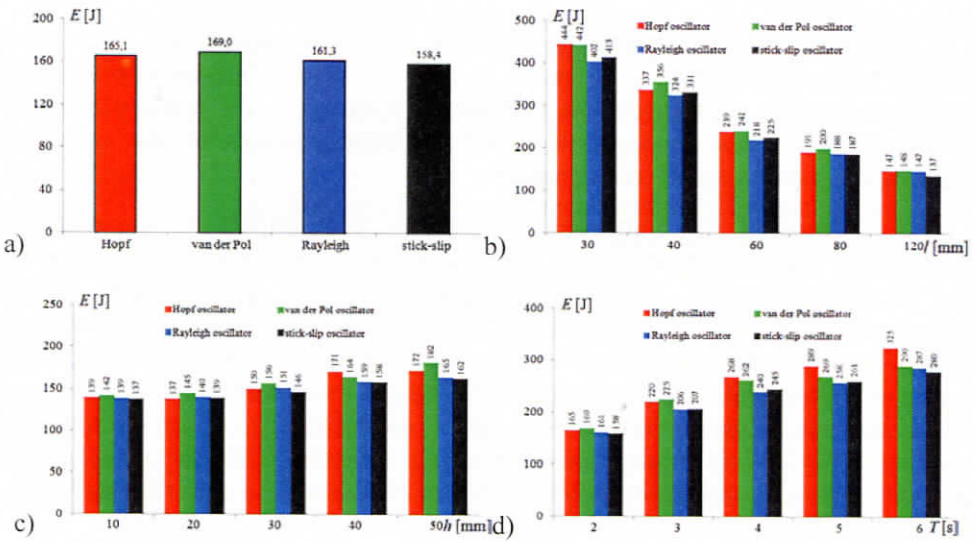

Fig. 8.20. Comparison of the total energy demand of the hexapod robot: a) for different CPG models, b) for different stride length l, c) for different stride height h, d) for different stride period T

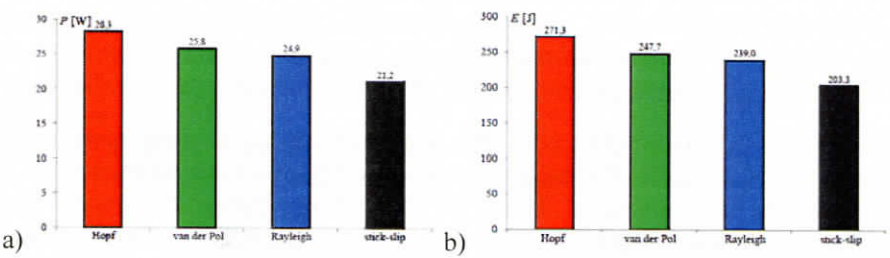

Fig. 8.21. Energetic analysis of the robot during transport additional mass 2.25 kg: a) average power consumption, b) total energy demand

8.7. Conclusions

A biologically-inspired prototype of the hexapod robot is investigated both numerically and experimentally by means of dynamical modelling of the robot, obtaining kinematic and dynamic parameters describing the robot locomotion

and some aspects of its power consumption analysis. The walking process of the robot with the tripod gait on a flat and hard ground is realized by four different CPG models and different stride parameters. Some interesting numerical simulations and experimental results regarding the whole robot are obtained, reported and discussed.

The proposed CPG model is relatively simple in comparison with other control methods presented in literature and it is sufficient especially when robot walks on the flat, regular surfaces. Moreover, both numerical and experimental results indicate some analogies between the characteristics of the simulated walking robot and animals met in nature.

The choice of the employed CPG has a great impact on the obtained kinematical and dynamical results. The CPG constructed based on the van der Pol oscillator appears to be the worst, since the greatest unnecessary accelerations and decelerations both in the vertical and horizontal (movement) direction of the robot are observed. The mentioned fluctuations of the gravity centre as well as unnecessary changes of speed and acceleration in the movement direction of the robot can have a great impact on the energy consumption during walking. This is why during normal walking both the variation curves of the gravity centre and acceleration of the robot in the movement direction should be possibly close to zero.

The numerically obtained and experimentally verified results of the study of the whole robot show that the proposed CPG has some advantages in comparison to other designs presented in this chapter. Namely, the robot controlled by the mentioned CPG does not have unnecessary fluctuations of the gravity centre and low acceleration/deceleration in moving direction. The obtained information can be used for further analysis of the strength and structural stability of the robot legs, trouble-free use as well as extension of life and operating time of the robot.

It should be also noted that the development of multi-legged walking machines is still restricted by the problem of their high power consumption. Due to the mentioned problem, a choice of the optimal robot movement can be applied to cover long distances by the robot in a more efficient way, especially on regular terrains. Finally, power efficiency optimization without improving of the power supply unit allows to increase the robot mission time.

Acknowledgments

The work has been supported by the Polish National Science Centre under the grant OPUS 9 no. 2015/17/B/ST8/01700 for years 2016-2018.

8.8. References

8.1 Arikawa K., Hirose S., Development of quadruped walking robot TITAN-VIII, IEEE International Conference on Intelligent Robots and Systems, 1996, pp. 208-214.

8.2 Berns K., Ilg W., Deck M., Dillmann R., The mammalian-like quadrupedal walking machine BISAM, Fifth International Workshop on Advanced Motion Control, 1998, pp. 429-433.

8.3 Chen J., Liu Y., Zhao J., Zhang H., Jin H., Biomimetic design and optimal swing of a hexapod robot leg, Journal of Bionic Engineering, Vol. 11, 2014, pp. 26-35.

8.4 Chen W., Ren G., Zhang J., Wang J., Smooth transition between different gaits of a hexapod robot via a central pattern generators algorithm, Journal of Intelligent & Robotic Systems, Vol. 67, 2012, pp. 255-270.

8.5 Chen X., Wang L., Ye X., Wang G., Wang H., Prototype development and gait planning of biologically inspired multi-legged crablike robot, Mechatronics, Vol. 23, 2013, pp. 429-444.

8.6 Cohen A., Holmes P., Rand R., The nature of the coupling between segmental oscillators of the lamprey spinal generator or locomotion: a mathematic model, Journal of Mathematical Biology, Vol. 13, 1982, pp. 345-369.

8.7 Delcomyn F., Neural basis of rhythmic behavior in animals, Science, Vol. 210, 1990, pp. 492-498.

8.8 Delcomyn F., Nelson M., Architectures for a biomimetic hexapod robot, Robotics and Autonomous Systems, Vol. 30, 2000, pp. 5-15.

8.9 Durr V., Schmitz J., Cruse H., Behaviour-based modelling of hexapod locomotion: linking biology and technical application, Arthropod Structure & Development, Vol. 33(3), 2004, pp. 237-250.

8.10 Fukuoka Y., Kimura H., Hada Y., Takase K., Adaptive dynamic walking of a quadruped robot 'Tekken' on irregular terrain using a neural system model, IEEE International Conference on Robotics and Automation, Vol. 2, 2003, pp. 2037-2042.

8.11 Galvez J., Estremera J., Gonzalez de Santos P., A new legged robot configuration for research in force distribution, Mechatronics, Vol. 13, 2003, pp. 907-932.

8.12 Grzelczyk D., Stańczyk B., Awrejcewicz J., Prototype, control system architecture and controlling of the hexapod legs with nonlinear stick-slip vibrations, Mechatronics, Vol. 37, 2016, pp. 63-78.

8.13 Grzelczyk D., Stańczyk B., Awrejcewicz J., Kinematics, dynamics and power consumption analysis of the hexapod robot during walking with tripod gait, International Journal of Structural Stability and Dynamics (accepted).

8.14 Ijspeert A., Central pattern generators for locomotion control in animals and robots: a review, Neural Network, Vol. 21(4), 2008, pp. 642-653.

8.15 Jin B., Chen C., Li W., Power consumption optimization for a hexapod walking robot, Journal of Intelligent & Robotic Systems, Vol. 71, 2013, pp. 195-209.

8.16 Klaassen B., Linnemann R., Spenneberg D., Kirchner F., Biomimetic walking robot SCORPION: control and modeling, Robotics and Autonomous Systems, Vol. 41, 2002, pp. 69-76.

8.17 McGhee R., Frank A., On the stability properties of quadruped creeping gaits, Mathematical Biosciences, Vol. 3, 1968, pp. 331-351.

8.18 Nishii J., Legged insects select the optimal locomotor pattern based on the energetic cost, Biological Cybernetics, Vol. 83, 2000; pp. 435-442.

8.19 Piątek M., Problems of the controlling walking robots - generators of the hexapod robot gaits, Doctoral Thesis, Krakov, AGH University of Science and Technology, 2012 (in Polish).

8.20 Raibert M., Blankespoor K., Nelson G., Rob playter and the BigDog Team, BigDog, the rough-terrain quadruped robot, The International Federation of Automatic Control, 2008, pp. 10822-10825.

8.21 Schilling M., Hoinville T., Schmitz J., Cruse H., Walknet, a bio-inspired controller for hexapod walking, Biological Cybernetics, Vol. 107, 2013, pp. 397-419.

8.22 Spenneberg D., Strack A., Hilljegerdes J., Zschenker H., Albrecht M., Backhaus T., et al., ARAMIES: a four-legged climbing and walking robot, Eighth International Symposium iSAIRAS, 2005.

8.23 Steingrube S., Timme M., Wörgötter F., Manoonpong P., Self-organized adaptation of a simple neural circuit enables complex robot behaviour, Nature Physics, Vol. 6, 2010, pp. 224-230.

8.24 Wang T., Guo W., Li M., Zha F., Sun L., CPG control for biped hopping robot in unpredictable environment, Journal of Bionic Engineering, Vol. 9, 2012, pp. 29-38.